



Assessment of CO₂ uptake on 13X zeolite by conducting batch and continuous fluidized tests

Amer A. Shneat^{a,*}, Raghad F. Almily^a, Dina R. Rzaij^b

^a Department of Chemical Engineering, College of Engineering, University of Baghdad, Baghdad, Iraq

^b Department of Chemical and Process Engineering, Faculty of Engineering and Built Environment, University of Kebangsaan Malaysia, 43600 Bangi, Malaysia

Abstract

The development of new, cleaner technologies is presently receiving a lot of attention to capture pollutant CO₂ gas. 13X zeolite is one of the most popular adsorbents employed for this purpose. Batch and continuous fluidized beds were used to examine the adsorption capacity. Isothermal and kinetic models for the batch were determined at 1–5 bar and 298 K and 303 K pressure range and temperatures, respectively. The Langmuir model fitted the process with $q_m = 4.01$ mmol/g and a correlation $R^2 = 0.986$. Pseudo-first order was also fitted with a correlation of $R^2 = 0.997$. The impact of the inlet CO₂ concentration (5%, 10%, and 14%), the bed heights varied between (5, 15, 25) cm, with a flow rate range of (6, 10, 14) L/min at temperature 298 K and pressure of 0.5 bar (gauge pressure), was investigated by utilizing the area under the breakthrough curve in a continuous fluidized bed experiment. Lower flow rate (6 l/m), bed height (25 cm), and higher CO₂ initial concentration (14%) achieved the best results.

Keywords: CO₂ capture; batch adsorption; isotherm study; kinetic study; continuous adsorption; breakthrough curve; fluidized bed.

Received on 04/05/2024, Received in Revised Form on 01/10/2024, Accepted on 06/10/2024, Published on 30/06/2025

<https://doi.org/10.31699/IJCPE.2025.2.11>

1- Introduction

Burning fossil fuels contributes to global warming and releases harmful pollutants into the atmosphere that can harm human health, including carbon dioxide, nitrogen dioxide, atmospheric ammonia, and polycyclic aromatic hydrocarbons [1, 2]. Assuming continuous increases in greenhouse gas emissions, the concentration of greenhouse gases in the atmosphere by the end of the century might be four times greater than pre-industrial levels [3].

Prioritizing the gradual substitution of ecologically benign energy sources for fossil fuels as the primary energy source has emerged [4]. Even though tremendous effort is currently being put toward developing new and cleaner technologies, like chemical looping combustion, new gasification technologies for power plants, and hydrogen-based fuel cells, adopting of appropriate post-combustion technologies can result in immediate and effective CO₂ mitigation. Growing interest is being shown in using porous materials for CO₂ capture within the context of the carbon capture and storage (CCS) strategy, to reduce short-term CO₂ industrial emissions [5].

Nowadays, amine-based absorption [6], membrane separation [7], cryogenic distillation [8], and adsorption [9] are among the methods used for the separation and capture of CO₂ gas.

Adsorbents need to possess a variety of characteristics in order to be able to extract CO₂ gas molecules from other gas combinations. The high surface area, porous

structure, and better selectivity are necessary to enhance adsorption capacity [10]. One of the most widely used adsorbents for this purpose is 13X zeolite [11, 12].

Industrial designs and units have effects that can be used in production activities. Although fluidized beds provide better heat and mass transfer rates than packed beds in many areas, there are additional technical barriers to their design and use [13]. Complete mixing of these particles with the flowing medium creates ideal conditions for efficient operation [14]. When a fluidized bed is used for adsorption, the adsorbed molecules can fully contact the adsorbent, which solves many common problems with packed bed adsorbents, including local temperature rise, bed clogging, uneven fluid distribution, and large bed pressure drop. [15].

Many studies were conducted on 13X zeolite for capturing CO₂. Girimonte et al. conducted an investigation into CO₂ adsorption on 13X zeolite pellets using a fluidized bed. The experiments compare the performance of a confined and conventional fluidized bed using the same apparatus at ambient temperature and pressure. The results showed that the confined bed has a higher adsorption capacity of 108 mg/g under 25 °C and 1 atm [16]. Khoramzadeh et al. studied the synthesis and isothermal analysis of zeolites 13X, 4A, 5A, and beta for CO₂ adsorption. They synthesized these zeolites using hydrothermal methods and characterized them using instrumental analysis techniques. The results showed that



*Corresponding Author: Email: amer.shneat1507D@coeng.uobaghdad.edu.iq

© 2025 The Author(s). Published by College of Engineering, University of Baghdad.

This is an Open Access article licensed under a [Creative Commons Attribution 4.0 International License](https://creativecommons.org/licenses/by/4.0/). This permits users to copy, redistribute, remix, transmit and adapt the work provided the original work and source is appropriately cited.

the highest adsorption capacity was found for zeolite 13X, while the lowest was found for zeolite beta. The Sips and Langmuir isotherm models were used to match the data, with the Sips model showing the best correlation [17]. Alibolandi et al. studied the separation of CO₂ gas from a mixture of CO₂/N₂ (80% N₂ and 20% CO₂) using the vacuum pressure swing adsorption (VPSA) process technique. Experiments were performed in an eight-step, four-bed setup using zeolite 13X and carbon molecular sieve (CMS) as adsorbents. A pressure range of 2.7–4.7 bar, cycle times of 360–600 s, the product flow rate of (1–3) L/min, and a temperature of 30 °C were the conditions employed. With 560 s for a cycle time of 3.7 bar, the maximum purity of 97.6% was obtained for the zeolite 13X adsorbent [18]. Fashi et al. conducted CO₂ capture adsorption on modified 13X zeolite with piperazine solution to examine adsorption capacity. The maximum adsorption capacity was obtained at a temperature of 25 °C, a pressure of 5 bar, a piperazine concentration of 2 wt.%, an adsorbent amount of 1 g, and a particle size of 200 μm. The adsorption capacity of Zeolite 13X increased from 193.844 to 242.084 mg/g after modification. The empirical isotherm data are more consistent with the Freundlich model. The best adsorption kinetic model was the Elovich model [19].

The aim of the present research is to investigate the adsorption capacity of 13X zeolite particles to adsorb CO₂ as well as to study the influence of operation mode, i.e., batch study on the adsorption isotherm and kinetics, and continuous study was performed in fluidized bed at various CO₂ concentrations, flow rates, and static bed heights. The research has focused on the comparison between the two modes of operation, i.e., the batch and continuous modes, and it did not focus on the type of adsorbent.

2- Theoretical aspects

2.1. Adsorption isotherm models

Langmuir isotherm: This model describes the performance of fluid-solid adsorption on zeolite. This theory proposed that the monolayer of adsorbed polluted fluid can be formed on a limited number of sites identically on equal locations without the interaction between neighboring adsorbed molecules. The model considers sorption to be uniform and the activation energy of sorption to be equal [20]. Many forms of Langmuir isotherm equations are found in the literature, and the linear one is [21]:

$$\frac{1}{q_e} = \frac{1}{q_m K_L C_e} + \frac{1}{q_m} \quad (1)$$

Freundlich Isotherm: assumes multilayer sorption on different sites and the surface is heterogeneous, many interactions between molecules take place due to different activation energies of molecules, the Freundlich linear equation is [21]:

$$q_e = \log K_F + \frac{1}{n} \log C_e \quad (2)$$

According to the Temkin [22] isotherm equation, adsorption is characterized by a uniform distribution of binding energies, and the heat of adsorption of all the molecules in the layer decreases linearly with coverage because of adsorbent-adsorbate interactions. The linear equation is [23]:

$$q_e = \beta_T \ln K_T + \beta_T \ln C_e \quad (3)$$

When the Gaussian energy disperses across a heterogeneous surface, the Dubinin-Kaganer-Radushkevich isotherm is typically employed [24]. According to Vijayaraghavan et al. [20] and Theivarasu and Mylsamy [25], the model is a semi-empirical equation that describes a pore-filling mechanism with implausible asymptotic behavior and is unable to predict Henry's law at low pressure. Also, according to Vijayaraghavan et al. [26], the model is utilized to differentiate between the chemisorption and physisorption of iron metal. The following depicts the Dubinin-Kaganer-Radushkevich isotherm model:

$$\ln q_e = \ln q_m - K_D \varepsilon^2 \quad (4)$$

ε is Dubinin-Kaganer-Radushkevich isotherm constant which can be determined using the equation below:

$$\varepsilon = RT \ln \left(1 + \frac{1}{C_e} \right) \quad (5)$$

2.2. Adsorption kinetics

For physical adsorption, the reversible interaction between the adsorbent and adsorbate was described by a pseudo-first-order equation. On the other hand, the chemical adsorption was mostly explored using the pseudo-second-order equation [27, 28]. A model of intraparticle diffusion is required in order to identify the rate-limiting phase that impacts the adsorption kinetics [29]. The pseudo-first order is given by Eq. 6:

$$\ln(q_e - q_t) = \ln q_e - K_1 t \quad (6)$$

The relation of pseudo-second order is expressed as:

$$\frac{t}{q_t} = \frac{1}{K_2 q_e^2} + \frac{t}{q_e} \quad (7)$$

The intra-particle model is represented by Eq. 8:

$$q_t = K_{in} t^{1/2} + C \quad (8)$$

The Elovich kinetic linear model [30] can also be utilized and represented by Eq. 9:

$$q_t = \frac{1}{\beta_E} \ln(\alpha \beta_E) + \frac{1}{\beta_E} \ln t \quad (9)$$

3- Experimental work

3.1. Batch apparatus

Fig. 1 illustrates the experimental setup of the adsorption equilibrium. Two tube vessels were utilized for this purpose with a volume of 0.5 L each; one of them was the reservoir, and the other was the adsorber, which

was made of iron. All fittings and tubes were made of 3/8 copper with 3 valves (V_1 , V_2 , and V_3) to control the flow of gas, and the rig was provided with a pressure gauge to measure the applied pressure. The temperature was to be controlled by using a hot plate (Dragon Lab, MS-H-Pro, China), and gas CO_2 was supplied from the cylinder (99.9% purity was purchased from Albilal Gas Company located in Baghdad), provided with a regulator. Also, a vacuum pump (vacuum pump, 2XZ-4, China) was used in the experiment.

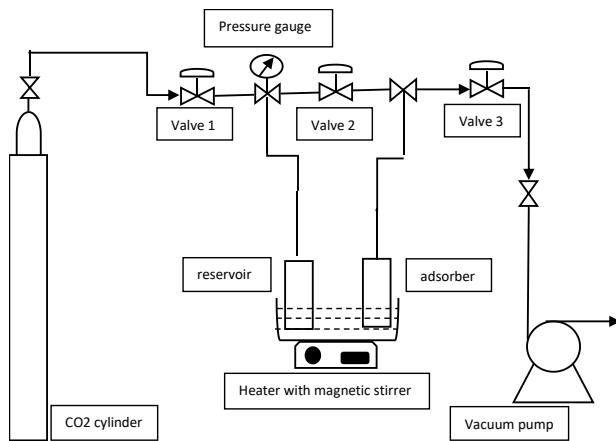


Fig. 1. Schematic diagram of batch adsorption apparatus

3.1.1. Method

Table 1 displays the features and technical specifications of the commercial zeolites 13X that were purchased from China and utilized in the experiment with particle density 1440 kg/m^3 [31]. To remove any moisture, the sample was first heated to 373 K for two hours. Also, prior to every measurement, the sample underwent one hour of degassing at 0.1 bar of vacuum.

Table 1. Technical characterizations of commercial zeolites 13X

Properties	Unit	Value
Particle diameter	Mm	0.4-0.8
Total Pore volume	cm^3/g	0.370
Surface area	m^2/g	786.38
Specific gravity	-	1.44
Moisture content	Wt %	≤ 0.5
Bulk density	Kg/m^3	650

For the isotherm test, through valve V_1 , carbon dioxide gas was injected into the reservoir chamber until the necessary pressure was obtained. When the value reached a steady state, V_1 was closed, and the pressure value was then recorded. then valve V_2 was opened, allowing gas to flow to the adsorber while valve V_3 was still closed, and then the second value was recorded after maintaining equilibrium. A mass balance is used for estimating the amount of adsorbed CO_2 gas at equilibrium to obtain the following equation [32].

$$q_e = \frac{[(C_1 - C_f)V_r - C_f \epsilon \cdot V_a]}{w} \quad (10)$$

For the kinetic test, valve V_1 was opened to allow gas CO_2 enter the reservoir vessel until it reaches a specific pressure value, then valve V_2 was opened to make gas expand into the adsorber vessel, using a timer to record pressure values every time interval till it reaches equilibrium. The amount of adsorbed CO_2 gas at time t can be given in the following equation [32].

$$q_t = \frac{[(C_1 - C_t)V_r - C_t \epsilon \cdot V_a]}{w} \quad (11)$$

3.2. Continuous experimental rig

The laboratory fluidized bed rig that was built for the CO_2 adsorption test from gas mixture CO_2/N_2 is schematically shown in Fig. 2. With an internal diameter of 40 mm and a height of 500 mm , the glass-type QVF column was outfitted with two 0.35 mm aperture sieves at both ends: the top and the bottom to regulate gas distribution and retain packing particles in place. Process conditions were measured with the installation of temperature sensors and pressure gauges. Gases entering and leaving the system are measured by flow meters. CO_2 and N_2 gas cylinders (were purchased from Albilal Gas Company located in Baghdad); they were the mixture of gases used in the experiment; each gas had a purity of 98% . The outlet CO_2 concentration was determined using a GEOTECH CO_2 analyzer (Geotechnical Instruments, BIOGAS 5000, United Kingdom).

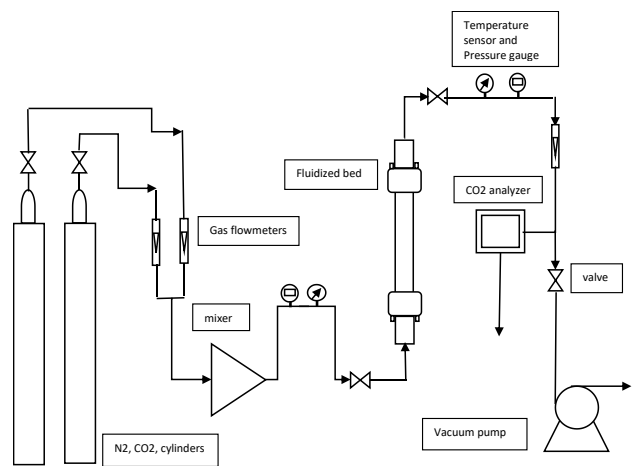


Fig. 2. Schematic diagram of experimental setup for CO_2 adsorption in fluidized bed

3.2.1. Method

In this experiment the particles used are group Geldart B, the minimum fluidization velocity U_{mf} for the solid particles has been calculated using Wen and Yu equation [33].

$$U_{mf} = \frac{\mu_g}{\rho_g d_p} \sqrt{(33.7)^2 + 0.0408 \frac{d_p^3 \rho_g (\rho_p - \rho_g) g}{\mu_g^2}} - 33.7 \quad (12)$$

For a given temperature and partial pressure of CO_2 , the specific equilibrium amount of adsorbed CO_2 can be

determined by integrating the breakthrough curve based on the following mass balance equation [34]:

$$q_{\text{ads}} = \frac{Q}{w} \int_{t=0}^{t=t} (C_0 - C_t) dt \quad (13)$$

The conditions for each adsorption experiment can be found in Table 2. The solid adsorbent had been heated to 373 K to eliminate any traces of moisture and CO₂ adsorbed molecules, and then it was exposed to argon gas prior to each run. In a typical experiment, the sorbent was loaded in the column to reach the desired bed height level.

Table 2. Experimental data

Experimental condition	Data
Bed height, H	5 cm, 15 cm, 25 cm
Column length, L	500 mm
Column diameter, D	40 mm
Inlet CO ₂ concentration, C ₀	5%, 10%, 14 %
Inlet flow rate, Q	6 L/m, 10 L/min, 14 L/min
Vacuum pressure	0.1 bar
Adsorption temperature, T	298 K
Total pressure, P	0.5 bar

A series of experiments were performed at a temperature 298 K and total pressure of 0.5 bar by employing many variables (bed height, flow rate, and initial concentration of CO₂), this process was carried out in a continuous operation method and the amount of carbon dioxide adsorbed was equivalent to the area under the breakthrough curve and through the use of the Eq. 13.

4- Results and discussion

4.1. Batch adsorption isotherm

Pure CO₂ gas was used only in the batch experiment, and the effects of both temperature and pressure were investigated.

According to Fig. 3, both isotherm curves show the same behavior irrespective of temperature, where the amount of CO₂ adsorbed on the adsorbent increases dramatically as equilibrium pressure rises above the low-pressure region before tending to stabilize as pressure rises further. The isotherm curve's quick rise indicated the ideal equilibrium pressure range, which supports the majority of adsorption activity. The curve's stabilized amount of CO₂ adsorbed indicates that CO₂ gas is occupying every adsorption site [35], signifying that the adsorbent's maximum capacity was obtained at 298 K and 5 bar.

Additionally, the impact of temperature on the CO₂ adsorption isotherm on the 13X zeolite was observed. Raising the operation temperature reduces both the capacity and the total amount adsorbed on the adsorbent. A rise in temperature from 298 K to 303 K made the total amount of the adsorbed CO₂ molecules unstable on the surface and increased the amount of CO₂ molecules that desorbed (a further increase in temperature resulted in a further decrease in capacity) because of the increase in molecule interactions and surface energy [36]. This is

consistent with the exothermic behavior of the 13X zeolite for CO₂ adsorption.

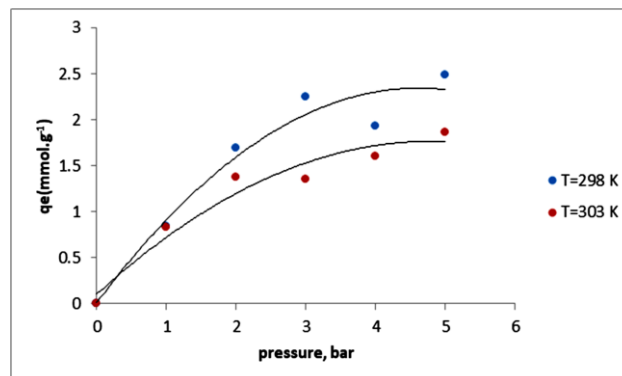


Fig. 3. Isotherm equilibrium curve relates CO₂ amount adsorbed and partial pressure 1-5 bar at 298 K and 303 K

To explain the experimental results of CO₂ adsorption on the surface of 13X zeolite, many isotherm models were used. Fig. 4 to Fig. 7, all illustrate the 13X zeolite isotherm models. According to data given in Table 3, Langmuir isotherm model was better for fitting the CO₂ adsorption data with a correlation value R² of 0.986, other models showed a lower correlation coefficient. Based on these results, it was believed that monolayer adsorption was applicable on an ideal surface and no interaction between the neighboring adsorbed molecules [37].

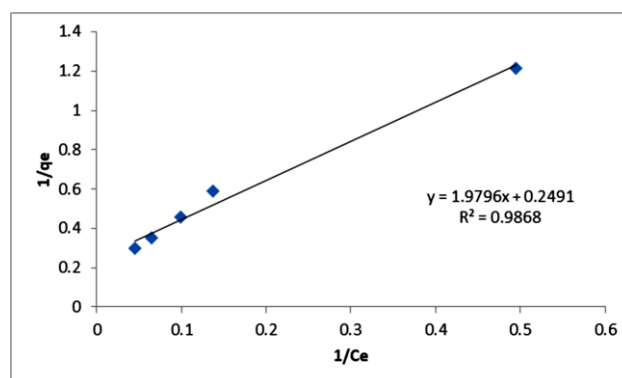


Fig. 4. Langmuir isotherm model

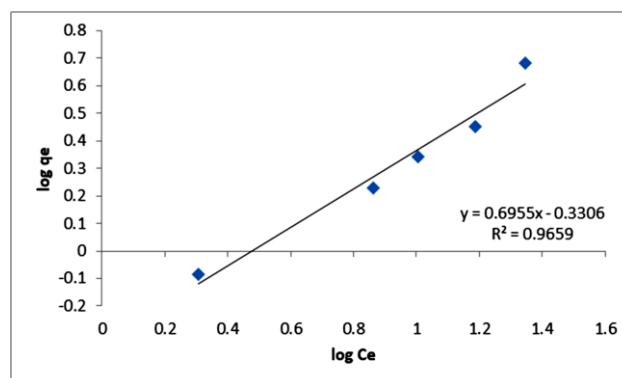


Fig. 5. Freundlich isotherm model

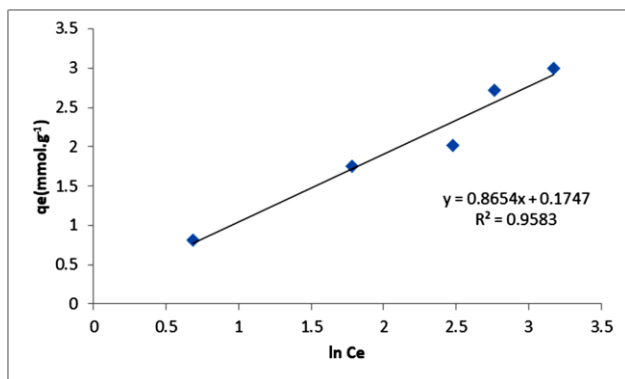


Fig. 6. Temkin isotherm model

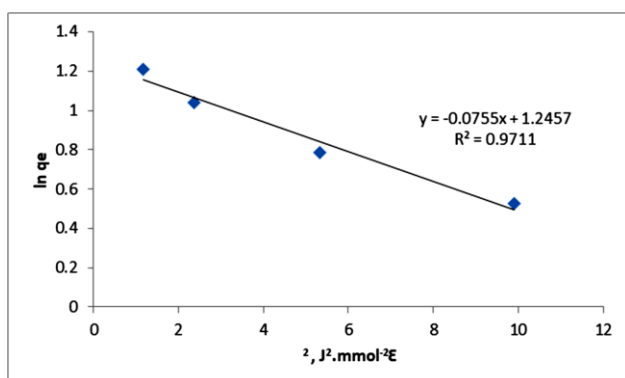


Fig. 7. Dubinin–Kaganer– Radushkevich isotherm model

Table 3. Isotherm equilibrium data at 298 K and 303 K

Model	Parameters	Temperature	
		298 K	303 K
Langmuir	q_m (mmol. g ⁻¹)	4.01	3.67
	K_L (L.mmol ⁻¹)	0.1259	0.1425
	R^2	0.986	0.989
Freundlich	K_F (mmole ^{1-1/n} . g)	0.467	0.602
	n (g.L ⁻¹)	1.437	1.91
	R^2	0.965	0.95
Temkin	K_T (L. mmol ⁻¹)	0.921	1.223
	β (J.mol ⁻¹)	1.0454	0.8654
	R^2	0.954	0.958
Dubinin–Kaganer–Radushkevich	q_D (mmol. g ⁻¹)	3.475	2.980
	K_D (mmol ² .J ⁻²)	0.0755	0.0386
	R^2	0.971	0.941

4.2. Batch adsorption kinetics

The rate of adsorption of the related adsorbent and adsorbate can be represented by adsorption kinetics. The reaction order and adsorption rate constant (k) obtained from the adsorption kinetics model consider an indication of the characteristics of adsorption. To estimate the CO₂ adsorption rate of 13X zeolite, the CO₂ adsorption kinetics data at different temperatures, 298 K, 303 K, under the pressure of 5 bar were obtained.

From Fig. 8 adsorption capacity in the time intervals decreases as the temperature increases at constant pressure. At the earlier stage of adsorption, it was noticed that carbon dioxide attracted quickly to the surface of bed particles, then it slowed down till it reached saturation.

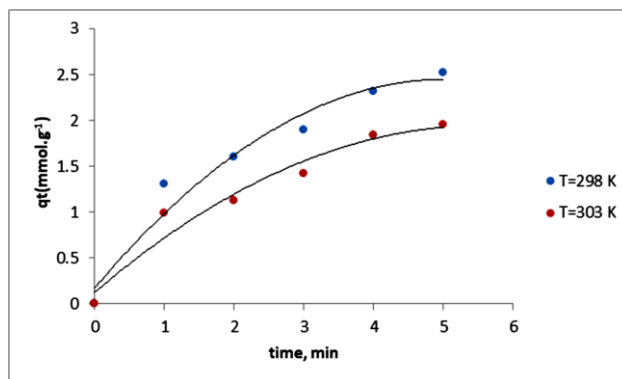


Fig. 8. Kinetic equilibrium curve relates CO₂ amount adsorbed and time for 5 bar at 298 K and 303 K

In the case of reaction models, due to Fig. 9 to Fig. 12, experimental data would be fitted with equations like pseudo-first order, pseudo-second order, intra-particle, and Elovich models, which helped in knowing the reaction order and rate constants. Table 4 shows that CO₂ adsorption taken at temperatures of 298 K and 303 K follows the rate controlling step of pseudo-first order, as it has the biggest coefficient correlation R^2 value [38].

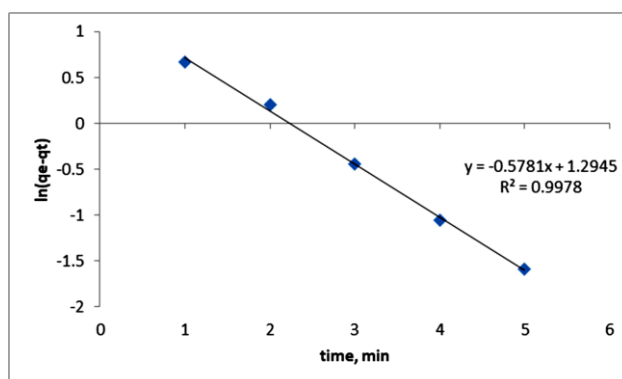


Fig. 9. Pseudo-First order model

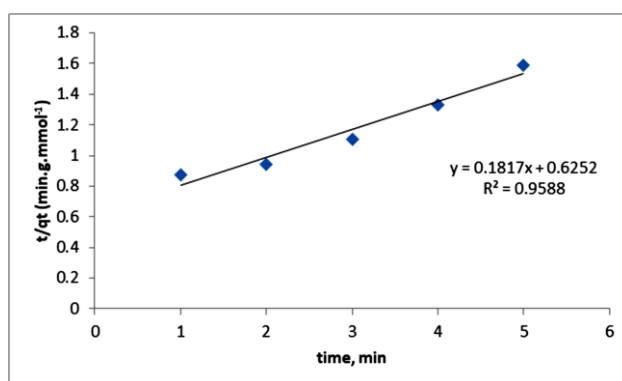


Fig. 10. Pseudo-Second order model

4.3. Continuous adsorption

To investigate the fluidization parameters of 13X zeolite utilized in the design rig and the effects of the main characteristics on the fluidization experiment. Tests were conducted under a constant temperature and pressure of 298 K and 0.5 bar. All results are shown in Table 5.

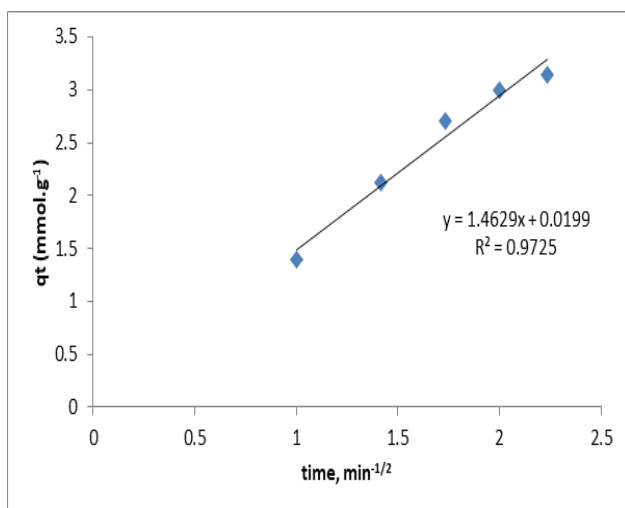


Fig. 11. Intra-particle kinetic model

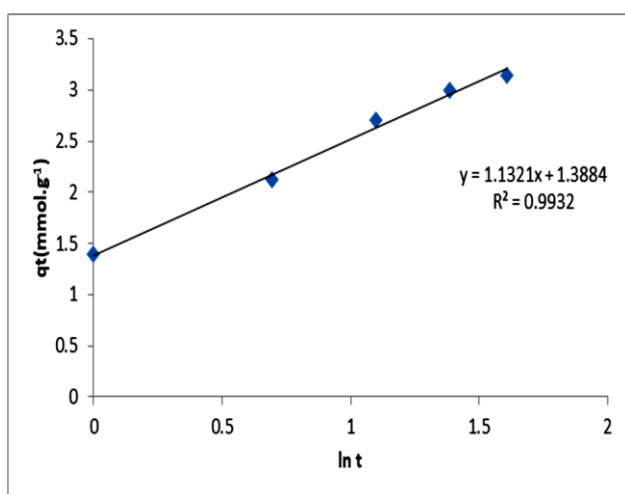


Fig. 12. Elovich kinetic model

Table 4. Kinetic equilibrium data at 298 K and 303 K

Model	Parameters	Temperature	
		298 K	303 K
pseudo-first order	q_e (mmol. g ⁻¹)	3.64	2.89
	K_1 (min ⁻¹)	0.5781	0.4786
	R^2	0.997	0.999
pseudo-second order	q_e (mmol. g ⁻¹)	5.5	4.61
	K_2 (g. min. mmol ⁻¹)	0.0528	0.0671
	R^2	0.958	0.972
Intra-particle	K_i (mmol.g ⁻¹ .min ^{-0.5})	1.4629	1.2343
	C	0.0199	0.0696
	R^2	0.972	0.98
Elovich	β (g. mmol ⁻¹)	0.8833	1.049
	α ((mmol.g ⁻¹ .min ⁻¹))	3.858	3.449
	R^2	0.993	0.997

4.3.1. Effect of flow rate

The breakthrough curves at a temperature of 298 K and a pressure of 0.5 bar, with flow rates of (6, 10, 14) L/min, bed height of 5 cm, and CO₂ concentration (14%) in the input gas stream were investigated in the tests using 13X zeolite. Fig. 13 illustrates how the breakthrough time in

the adsorption column decreased as the flow rate increased. The breakthrough time varied significantly, starting at 60 seconds, and the saturation time for 6 L/min has occurred at 160 seconds. As the flow rate increased to 14 L/min, the saturation was reached earlier. Analyzing how the gas flow rate affects process performance and finding that a higher flow rate causes the breakthrough curve to achieve a steady state more quickly. That phenomenon was most likely caused by an increase in the gas–solid contact for flow rate 14 L/min; in other words, the rapid mass transfer could be the cause of the short breakthrough time [39]. By raising the flow rate, the saturation time (steeper curve) was shortened, and by using data obtained and applying equation 13, the capacity was smaller as illustrated in Table 5.

4.3.2. Effect of bed height

The experiment followed the same parameters as shown in Fig. 14, with the exception that the flow rate was kept constant at 6 L/m and the bed heights varied between 5, 15, and 25 cm. The breakthrough curve for the bed 25 cm showed a beneficial trend; it started at around 180 s and terminated at 350 s. The saturation was decreased by following the arrangements 25 cm, 15 cm, and 5 cm, where the gas moved faster. This indicated that before the breakthrough, a significant portion of the particles were exposed to CO₂ right away. This can be interpreted by the homogeneity provided to the particles due to fluidization [40]. To capture CO₂ molecules, there has to be a larger open surface area in contact with the gas as the amount of adsorbent increases. By applying equation 13 using data C/C_0 vs. time, the amount adsorbed was enhanced as the bed became heavier, that is, the adsorption capacity became higher, as indicated in Table 5.

4.3.3. Effect of initial concentration

Since the moment the gas mixture started to flow from the fluidized bed to the analyzer, data on CO₂ concentration were presented as a function of time (breakthrough curve). Fig. 15 shows the effect of the inlet CO₂ concentration 5%, 10%, and 14% on the breakthrough curve with a constant flow rate of 6 L/min and a bed height of 5 cm. As was seen from Fig. 15, breakthrough time became shorter as the inlet concentration increased. The number of CO₂ molecules available per unit volume of feed increased positively with the rise in the inlet CO₂ concentration. Because of this, a greater concentration gradient between the gaseous and solid phases developed, which sped up the adsorbent bed's saturation by facilitating the mass transfer of CO₂ molecules from the feed to the porous adsorbent sites. Furthermore, as demonstrated by the rise in adsorption capacity of adsorbents in Table 5, an increase in the inlet CO₂ concentration led to a larger uptake of CO₂ molecules. This might be because of the higher concentration gradient, which gave gas molecules more of a driving force to overcome their mass transfer resistance and result in a larger uptake [41, 42].

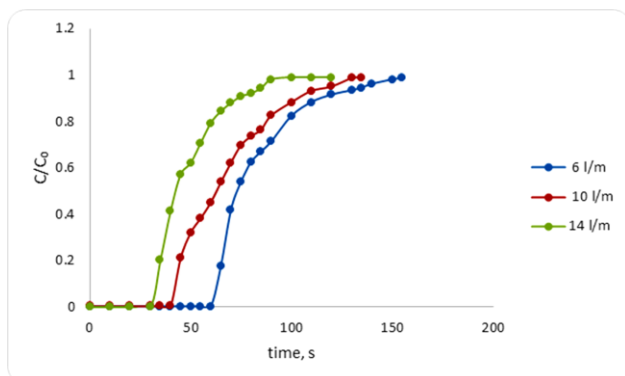


Fig. 13. Breakthrough curve for 5 cm bed height, 14 % CO₂ concentration with different flow rates at 298 K and 0.5 bar

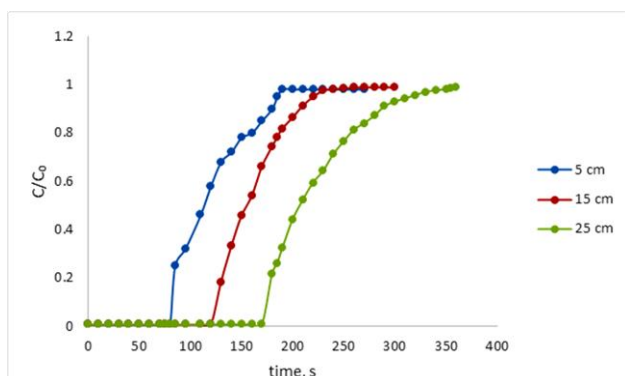


Fig. 14. Breakthrough curve for 6 L/m flow rate, 14 % CO₂ concentration with different bed heights at 298 K and 0.5 bar

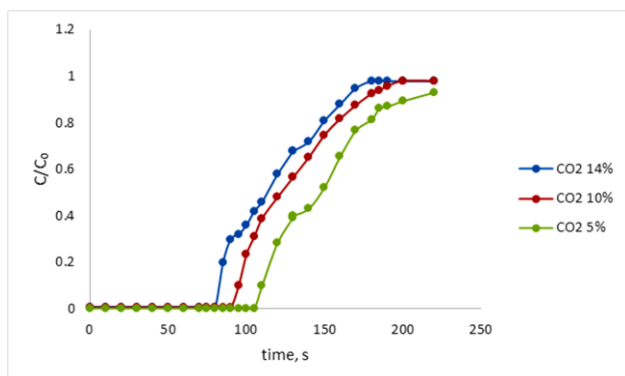


Fig. 15. Breakthrough curve for 6 L/m flow rate, 5 cm bed height with different CO₂ concentrations at 298 K and 0.5 bar

Table 5. Variables and uptake data at 298 K and 0.5 bar

Ini. Concentration %	Q (L/min)	H (cm)	q _{ads} (mmol/g)
5	6	5	0.94
10	6	10	1.71
14	6	14	2.25
14	10	14	1.9
14	14	14	1.47
14	6	14	2.98
14	6	14	4.1

5- Conclusion

An isotherm and kinetic studies were conducted on CO₂ adsorption on 13X zeolite. Langmuir had the best correlation coefficient with $R^2 = 0.986$ at 298 K and 5 bar among other models, Freundlich, Temkin, and Dubinin-Kaganer-Radushkevich, which proved the monolayer distribution of molecules on an ideal surface. It was noticed that the saturation adsorption capacity of CO₂ from the mixture of N₂ and CO₂ increased appreciably with decreased bed temperatures. The saturation adsorption capacity rose from 3.67 to 4.01 mmol/g, with a decrease in bed temperature from 303 K to 298 K. The kinetic models used were pseudo-first-order, pseudo-second-order, intra-particle, and Elovich models. The best performance was conducted at 298 K. The rate-controlling step was described by pseudo-first-order, as the correlation coefficient R^2 was 0.997 at 298 K and 0.999 at 303 K.

Another set of experiments was conducted using continuous mode by studying the behavior of the breakthrough curve in a fluidized bed at a temperature of 298 K and a pressure of 0.5 bar (low pressure), utilizing factors such as bed height, flow rate, and initial CO₂ concentration. A slow flow rate, increased bed height, and increased CO₂ concentration were found to enhance adsorption capacity. The best results were $q = 4.1$ mmol/g, obtained by 14% initial concentration, 25 cm bed depth, and a 6 l/m flow rate. With these ranges employed for the breakthrough test, the most effective parameter on adsorption capacity was bed height (bed weight), which explained that the employment of a fluidized bed enhanced the adsorption of CO₂ due to more surface exposure to better gas-solid contact.

Nomenclature

symbol	Meaning	Unit
1/n	Adsorption intensity	L.g ⁻¹
C	The intercept	-
C ₀	CO ₂ concentration at the inlet of the column	mmol. L ⁻¹
C _e	Equilibrium concentration of adsorbate	mmol. L ⁻¹
C _f	Final concentrations	mmol. L ⁻¹
C _i	Initial concentration	mmol. L ⁻¹
C _t	CO ₂ concentration at time t	mmol. L ⁻¹
d _p	Particle diameter	M
g	Gravitational acceleration	m.s ⁻²
K ₁	Rate constant of pseudo-first order adsorption	min ⁻¹
K ₂	Rate constant of pseudo-second order adsorption	g. min. mmol ⁻¹
K _D	Activity coefficient related to mean sorption energy	mmol ² .J ⁻²
K _F	Freundlich isotherm constant	mmole ^{1-1/n} .g
K _{in}	Intra-particle diffusion rate constant	mmol.g ⁻¹ .min ^{-0.5}
K _L	Langmuir isotherm constant	L. mmol ⁻¹

K_T	Temkin binding constant	L.mmol ⁻¹
Q	Volumetric flow rate at the inlet of column	L.min ⁻¹
q_{ad}	Adsorption capacity of the adsorbent	mmol. g ⁻¹
q_e	Adsorption capacity at equilibrium	mmol. g ⁻¹
q_m	Maximum adsorption capacity	mmol. g ⁻¹
q_t	Adsorption capacity at time t.	mmol. g ⁻¹
t	Time	Min
V_a	Adsorber volume	L
V_r	Reservoir volume	L
W	weight of the adsorbent in adsorber vessel	G
w	Mass of the adsorbent	G
α	Elovich initial sorption rate	mmol. g ⁻¹ .min ⁻¹
β_T	Temkin heat of adsorption	J.mol ⁻¹
β_E	Elovich constant related to the extent of surface coverage and activation energy for chemisorption	g. mmol ⁻¹
ϵ	Dubinin–Kaganer– Radushkevich isotherm constant	J. mmol ⁻¹
ϵ_o	Over all bed void fraction	-
μ_g	Gas viscosity	kg. m ⁻¹ . s ⁻¹
ρ_g	Density of gas	kg.m ⁻³
ρ_p	Density of particles	kg.m ⁻³

References

- [1] F. Perera, A. Ashraf, P. Kinney, and D. Mills, "Towards a fuller assessment of benefits to children's health of reducing air pollution and mitigating climate change due to fossil fuel combustion", *Environmental Research.*, vol. 172, pp. 55–72, 2019. <https://doi.org/10.1016/j.envres.2018.12.016>
- [2] F. Perera, "Pollution from fossil-fuel combustion is the leading environmental threat to global pediatric health and equity: solutions exist", *International Journal of Environmental Research and Public Health*, 15:16, 2018. <https://doi.org/10.3390/ijerph15010016>
- [3] M. H. Eldesouki, A. E. Rashed, and A. Abd El-Moneim, "A comprehensive overview of carbon dioxide, including emission sources, capture technologies, and the conversion into value-added products", *Clean Technologies and Environmental Policy*, vol. 25, pp. 3131–3148, 2023. <https://doi.org/10.1007/s10098-023-02599-9>
- [4] G. A. Mohammed and A. A. Shneat, "Parameters Affecting the Thermodynamic Efficiency of PEM Single Cell and Stack of Cells (Two Cells)", *Iraqi Journal of Chemical and Petroleum Engineering*, vol. 17 (3), pp. 91- 100, 2016. <https://doi.org/10.31699/IJCPE.2016.3.8>
- [5] T. Mendiara, F. García-Labiano, A. Abad, P. Gayán, L. F. de Diego, M. T. Izquierdo, and J. Adánez, "Negative CO₂ emissions through the use of biofuels in chemical looping technology: A review", *Applied Energy*, vol. 232, pp. 657-684, 2018. <https://doi.org/10.1016/j.apenergy.2018.09.201>
- [6] Z. L. Ooi, P. Y. Tan, L. S. Tan, and S. P. Yeap, "Amine-based solvent for CO₂ absorption and its impact on carbon steel corrosion: A perspective review", *Chinese journal of chemical engineering*, vol. 28(5), pp. 1357-1367, 2020. <https://doi.org/10.1016/j.cjche.2020.02.029>
- [7] G. Chen, T. Wang, G. Zhang, G. Liu, and W. Jin, "Membrane materials targeting carbon capture and utilization", *Advanced Membranes*, vol. 2, 100025, 2022. <https://doi.org/10.1016/j.advmem.2022.100025>
- [8] S. N. Zuraidi and H. Husin, "A Comparative Analysis Of Cryogenic, Adsorption And Amine-Based Absorption Techniques For Co₂ Capture", *Platform: A Journal of Engineering*, vol. 7(4), 2023. <https://doi.org/10.61762/pajevol7iss4art25235>
- [9] B. I. Waisi, J. T. Majeed and N. S. Majeed, "Carbon dioxide capture using nonwoven activated carbon nanofiber", *Earth and Environmental Science*, vol. 779, 2021. <https://doi.org/10.1088/1755-1315/779/1/012056>
- [10] N. Abuelnoor, A. AlHajaj, M. Khaleel, L. F. Vega, M. R. M. Abu-Zahra, "Activated carbons from biomass-based sources for CO₂ capture applications", *Chemosphere*, vol. 282, pp. 131111, 2021. <https://doi.org/10.1016/j.chemosphere.2021.131111>
- [11] S. M. Al-Jubouri, "The static aging effect on the seedless synthesis of different ranges Faujasite-type zeolite Y at various factors", *Iraqi Journal of Chemical and Petroleum Engineering*, vol. 20(4), pp. 7-13, 2019. <https://doi.org/10.31699/IJCPE.2019.4.2>
- [12] J. T. Majeed and N. S. Majeed, "Taguchi Design Methodology for the Optimization of CO₂ Permeance in Gas Capture Process from Polluted Air", *Environmental Earth Sciences*, vol. 1215, 2023. <https://doi.org/10.1088/1755-1315/1215/1/012010>
- [13] Y. Lv, Q. Sun, J. Li, W. Zhange, Y. He, and Y Zhou, "Disability Status and Its Influencing Factors Among Stroke Patients in Northeast China: A 3-Year Follow-Up Study", *National Library of Medicine*, vol. 17, pp. 2567-2573, 2021. <https://doi.org/10.2147/NDT.S320785>
- [14] S. M. Okhovat-Alavian, J. Behin, and N. Mostoufi, "Investigating bubble dynamics in a semi-cylindrical gas-solid fluidized bed", *Powder Technology*, vol. 370, pp. 129-136, 2020. <https://doi.org/10.1016/j.powtec.2020.05.032>
- [15] S. K. Govindarajan, A. Mishra, and A. Kumar, "Darcy's Experimental Empirical Relation and its Extension". *LARHYSS JOURNAL*, vol. 42, pp. 7-22, 2020.

- [16] R. Girimonte, B. Formisani, and F. Testa, "Adsorption of CO₂ on a confined fluidized bed of pelletized 13X zeolite", *Powder Technology*, vol. 311, pp. 9-17, 2017. <https://doi.org/10.1016/j.powtec.2017.01.033>
- [17] E. Khoramzadeh, M. Mofarahi, K. Chungand, and C.-H. Lee, "Equilibrium Adsorption Study of CO₂ and N₂ on Synthesized Zeolites 13X, 4A, 5A, and Beta", *Journal of Chemical & Engineering Data*, vol. 64 (12), 2019. <https://doi.org/10.1021/acs.jced.9b00690>
- [18] M. Alibolandi, S. M. Sadrameli, F. Rezaee, and J. T. Darian, "Separation of CO₂/N₂ mixture by vacuum pressure swing adsorption (VPSA) using zeolite 13X type and carbon molecular sieve adsorbents", *Heat and Mass Transfer*, vol. 56, pp. 1985-1994, 2020. <https://doi.org/10.1007/s00231-020-02823-y>
- [19] F. Fashi, A. Ghaemi, and A. H. Behroozi, "Piperazine impregnation on Zeolite 13X as a novel adsorbent for CO₂ capture: experimental and modeling", *Chemical Engineering Communications*, vol. 208(24), pp.1-17, 2021. <https://doi.org/10.1080/00986445.2020.1746657>
- [20] Aloko, D. F., and Eyitayo Amos Afolabi. "Titanium dioxide as a cathode material in a dry cell." *Leonardo Electronics Journal of Practices and Technologies*, vol. 11, pp. 97-108, 2007.
- [21] B. Guo, L. Chang, and K. Xie, "Adsorption of carbon dioxide on activated carbon", *Journal of Natural Gas Chemistry*, vol. 15, pp. 223-229, 2006. [https://doi.org/10.1016/S1003-9953\(06\)60030-3](https://doi.org/10.1016/S1003-9953(06)60030-3)
- [22] Temkin M.I., "Adsorption Equilibrium and the Kinetics of Processes on Nonhomogeneous Surfaces and in the Interaction between Adsorbed Molecules", *Russian Journal of Physical Chemistry A*, vol. 15, pp. 296-332, 1941.
- [23] J. S. Piccin, G. Dotto, and L. A. A. PINTO, "Adsorption isotherms and thermochemical data of FD and C RED N° 40 Binding by chitosan", *Brazilian Journal of Chemical Engineering*, vol. 28(2), pp. 295-304, 2011. <https://doi.org/10.1590/S0104-66322011000200014>
- [24] O. Çelebi, Ç. Üzümlü, T. Shahwan, and H.N. Erten, "A radiotracer study of the adsorption behavior of aqueous Ba²⁺ ions on nanoparticles of zero-valent iron", *Journal of Hazardous Materials*, vol. 148(3), pp. 761-767, 2007. <https://doi.org/10.1016/j.jhazmat.2007.06.122>
- [25] K. Vijayaraghavan, T.V.N. Padmesh, K. Palanivelu, and M. Velan, "Biosorption of nickel (II) ions onto Sargassum wightii: Application of two parameter and three-parameter isotherm models", *Journal of hazardous materials*, vol. 133(1-3), pp. 304-308, 2006. <https://doi.org/10.1016/j.jhazmat.2005.10.016>
- [26] C. Theivarasu, and S. Mysamy, "Removal of malachite green from aqueous solution by activated carbon developed from cocoa (Theobroma Cacao) shell-A kinetic and equilibrium studies", *E-Journal of Chemistry*, vol. 8(S1), pp. S363-S371, 2011. <https://doi.org/10.1155/2011/714808>
- [27] C. Goel, H. Kaur, H. Bhunia, and P.K. Bajpai, "Carbon dioxide adsorption on nitrogen enriched carbon adsorbents: experimental, kinetics, isothermal and thermodynamic studies", *Journal of CO₂ Utilization*, vol. 16, pp. 50-63, 2016. <https://doi.org/10.1016/j.jcou.2016.06.002>
- [28] M. H. Mohammed Ali, R. F. Almilly, and R. K. Abid, "Isotherms and Kinetics Study for Adsorption of Nitrogen from Air using Zeolite Li-LSX to Produce Medical Oxygen", *Iraqi Journal of Chemical and Petroleum Engineering*, vol. 24 (2), pp. 81-87, 2023. <https://doi.org/10.31699/IJCPE.2023.2.9>
- [29] W. J. Weber and J. C. Morris, "Kinetics of adsorption on carbon from solution", *Journal of the Sanitary Engineering Division*, vol. 89, pp. 31-60, 1963. <https://doi.org/10.1061/JSEDAI.0000430>
- [30] R. S. Juang, and M.L. Chen, "Application of the Elovich equation to the kinetics of metal sorption with solvent-impregnated resins", *Industrial & Engineering Chemistry Research*, vol. 36(3), pp. 813-820, 1997. <https://doi.org/10.1021/ie960351f>
- [31] R. Girimonte, B. Formisani, and F. Testa, "Adsorption of CO₂ on a confined fluidized bed of pelletized 13X zeolite", *Powder Technology*, vol. 311, pp. 9-17, 2017. <https://doi.org/10.1016/j.powtec.2017.01.033>
- [32] M. J. Ahmed and S. K. Theydan, "Isotherms and thermodynamics studies for binary adsorption of methane and ethane on 4A molecular sieve zeolite", *Journal of Porous Materials*, vol. 21, pp. 303-310, 2014. <https://doi.org/10.1007/s10934-013-9775-2>
- [33] S. E. Ebrahim and F. A. Rasheed, "Removal of Copper Ions onto Walnut Shells by Using Batch and Continuous Fluidized Bed", *Journal of Engineering*, vol. 19 (08), 2013. <https://doi.org/10.31026/j.eng.2013.08.04>
- [34] H. Chang, Z. Wu, M. Yao, S. Guo, "Experimental Investigation and Modeling of Adsorption of Carbon Dioxide on 5A Molecular Sieve for Helium Purification of High-Temperature Gas-cooled Reactor", *Energy Procedia*, vol. 39, pp. 208-226, 2012. <https://doi.org/10.1016/j.egypro.2013.07.208>
- [35] A. I. Sarker, A. Aroonwilas, and A. Veawab, "Equilibrium and Kinetic Behavior of CO₂ Adsorption onto Zeolites, Carbon Molecular Sieve and Activated Carbons", *Energy Procedia*, vol. 114, pp. 2450 - 2459, 2017. <https://doi.org/10.1016/j.egypro.2017.03.1394>
- [36] J. Shabanian and J. Chaouki, "Effects of temperature, pressure, and interparticle forces on the hydrodynamics of a gas-solid fluidized bed", *Chemical Engineering Journal*, vol. 313, pp. 580-590, 2017. <https://doi.org/10.1016/j.cej.2016.12.061>
- [37] E. Khoramzadeh, M. Mofarahi, and C. Lee, "Equilibrium Adsorption Study of CO₂ and N₂ on Synthesized Zeolites 13X, 4A, 5A, and Beta", *Journal of Chemical and Engineering*, vol. 64, pp. 5648-5664, 2019. <https://doi.org/10.1021/acs.jced.9b00690>

- [38] A. I. Sarkera, A. Aroonwilasa, and A. Veawab, "Equilibrium and Kinetic Behaviour of CO₂ Adsorption onto Zeolites, Carbon Molecular Sieve and Activated Carbons", *Energy Procedia*, vol. 114, pp. 2450–2459, 2017. <https://doi.org/10.1016/j.egypro.2017.03.1394>
- [39] J. Hedlund, G. Garcia, M. Balsamo, M. Zhou, and J. Mouzon, "Microchannel zeolite 13X adsorbent with high CO₂ separation performance", *Separation and Purification Technology*, vol. 277, 119483, 2021. <https://doi.org/10.1016/j.seppur.2021.119483>
- [40] N. S. Majeed and S. A. Alwan, "Study the Performance of Low Cost Material (Peanut Hulls) for Dye Adsorption Using Inverse Fluidized Bed", *Iraqi Journal of Chemical and Petroleum Engineering*, vol.15 (2), pp. 15- 25, 2014. <https://doi.org/10.31699/IJCPE.2014.2.3>
- [41] M. Auta and B.H. Hameed, "Preparation of waste tea activated carbon using potassium acetate as an activating agent for adsorption of Acid Blue 25 dye", *Chemical Engineering Journal*, vol. 171(2), pp. 502–509, 2011. <https://doi.org/10.1016/j.cej.2011.04.017>
- [42] M. Auta and B.H. Hameed, "Adsorption of carbon dioxide by diethanolamine activated alumina beads in a fixed bed", *Chemical Engineering Journal*, vol. 253, pp. 350–355, 2014. <https://doi.org/10.1016/j.cej.2014.05.018>

تقييم أمتصاص ثاني اوكسيد الكربون على الزيولايت 13X عن طريق إجراء أختبارات الطبقة الدفعية والطبقة المميعة المستمرة

عامر عبدالخضر شنيت^{١*}، رعد فريد قاسم الملي^١، دينا رحيم رزيح^٢

^١ قسم الهندسة الكيماوية، كلية الهندسة، جامعة بغداد، العراق

^٢ قسم الهندسة الكيماوية وهندسة العمليات، كلية الهندسة والبيئة المبنية، جامعة كيبانجان ماليزيا، ٤٣٦٠٠ بانجي، ماليزيا

الخلاصة

تُكرس حاليًا العديد من الجهود لتطوير تقنيات جديدة ونظفية لالتقاط غاز ثاني أوكسيد الكربون الملوث. يعد الزيولايت 13X واحدًا من أشهر المواد المازة المستخدمة لهذا الغرض. تم استخدام الطبقة الدفعية والطبقة المستمرة لفحص قدرة الامتزاز. تم تحديد موديلات تساوي الحرارة والحركية للطبقة الدفعية عند درجات حرارة ٢٩٨ كلفن و ٣٠٣ كلفن، وضغوط تتراوح بين ١-٥ بار، حيث تطابق موديل لانغماير مع نتائج العملية بمقدار ساعة=٤,٠١ ملي مول / غم وبمعامل دقة = ٠,٩٨٦ ، بينما تطابق موديل تفاعل المرتبة الاولى الزائف بمعامل دقة = ٠,٩٩٧. ايضا تم دراسة تأثير تركيز ثاني أوكسيد الكربون بنسب (٥%، ١٠%، ١٤%)، وباستخدام ارتفاعات الطبقة بين (٥، ١٥، ٢٥) سم، وبمدى معدل تدفق (٦، ١٠، ١٤) لتر/دقيقة تحت درجة الحرارة ٢٩٨ كلفن وضغط ٠,٥ بار، من خلال استخدام مساحة المنطقة الواقعة تحت منحنى الاحتراق في تجارب الطبقة المميعة المستمرة. حقق معدل التدفق المنخفض (٦ لتر/م^٣)، وارتفاع السرير (٢٥ سم)، والتركيز الأبتدائي لثاني أوكسيد الكربون (١٤%) أفضل النتائج.

الكلمات الدالة: احتجاز ثاني أوكسيد الكربون، امتزاز الطبقة الدفعية، دراسة التساوي الحراري، دراسة حركية الامتزاز، امتزاز الطبقة المستمر، منحنى الاحتراق، الطبقة المميعة.